

PNNL-35098

# A Lithium Feedstock Pathway: Coupled Electrochemical Saltwater Extraction and Direct Battery Materials Manufacturing

September 2023

Dongping Lu  
Matthew Asmussen

## DISCLAIMER

This report was prepared as an account of work sponsored by an agency of the United States Government. Neither the United States Government nor any agency thereof, nor Battelle Memorial Institute, nor any of their employees, makes **any warranty, express or implied, or assumes any legal liability or responsibility for the accuracy, completeness, or usefulness of any information, apparatus, product, or process disclosed, or represents that its use would not infringe privately owned rights.** Reference herein to any specific commercial product, process, or service by trade name, trademark, manufacturer, or otherwise does not necessarily constitute or imply its endorsement, recommendation, or favoring by the United States Government or any agency thereof, or Battelle Memorial Institute. The views and opinions of authors expressed herein do not necessarily state or reflect those of the United States Government or any agency thereof.

PACIFIC NORTHWEST NATIONAL LABORATORY  
*operated by*  
BATTELLE  
*for the*  
UNITED STATES DEPARTMENT OF ENERGY  
*under Contract DE-AC05-76RL01830*

Printed in the United States of America

Available to DOE and DOE contractors from  
the Office of Scientific and Technical Information,  
P.O. Box 62, Oak Ridge, TN 37831-0062

[www.osti.gov](http://www.osti.gov)

ph: (865) 576-8401

fox: (865) 576-5728

email: [reports@osti.gov](mailto:reports@osti.gov)

Available to the public from the National Technical Information Service  
5301 Shawnee Rd., Alexandria, VA 22312

ph: (800) 553-NTIS (6847)

or (703) 605-6000

email: [info@ntis.gov](mailto:info@ntis.gov)

Online ordering: <http://www.ntis.gov>

# **A Lithium Feedstock Pathway: Coupled Electrochemical Saltwater Extraction and Direct Battery Materials Manufacturing**

September 2023

Dongping Lu  
Matthew Asmussen

Prepared for  
the U.S. Department of Energy  
under Contract DE-AC05-76RL01830

Pacific Northwest National Laboratory  
Richland, Washington 99354

## Abstract

Lithium (Li) is one of the critical industrial materials and an indispensable component in manufacturing Li batteries. However, Li resource is limited and geographically uneven in earth's crust and its mining is not sustainable due to the low efficiency and complicated separation and refining processes. In this work, we develop a one-step technology to electrochemically extract Li from low concentration solutions (brines, seawater or used Li-ion batteries) into a form to directly produce commercial battery materials, eliminating the costly Li separation/purification steps. By using this approach, Li was selectively extracted and converted into battery cathodes (e.g., spinel  $\text{LiMn}_2\text{O}_4$  and layered  $\text{LiNi}_x\text{Mn}_y\text{Co}_z\text{O}_2$ ) through heat treatment. With the importance of Li-ion batteries to the overall decarbonization strategy, the demonstration of a one-step Li-extraction to a ready-to-use material could expand the access to Li resources at a lower cost by eliminating processing steps.

## Summary

A combined Li extraction-utilization technology was developed to realize efficient Li recovery from Li-containing aqueous solutions for direct cathode preparation without processes of Li separation and refinement. By eliminating the interferences of  $H^+$  and other metal cations through this approach, Li can be selectively extracted and inserted into EMD host, generating a chemically pure Li and Mn resource. High Li recovery efficiency of 0.772 Li/EMD was achieved. Instead of requiring post-processing Li separation or Li-host regeneration, the harvested Li along with the EMD can be used directly for Li battery cathode production. The synthesized spinel  $LiMn_2O_4$  and NMC333 were pure in phase structure and exhibit decent electrochemical performance as promising cathode materials. Significant benefits of using this technical loop for Li recovery and utilization include selective Li extraction, eliminated post-treatment, and high efficiency, which are desirable for industrial deployment. The Li-extraction flow cell with large working area was designed, manufactured, and demonstrated for continuous operation. This Li recovery and utilization technology could be expected to help address the existing challenges of Li shortage and battery cost, supporting the vehicle electrification and decarbonization of socioeconomic system.

## Acknowledgments

This research was supported by the **Strategic Investment** under the Laboratory Directed Research and Development (LDRD) Program at Pacific Northwest National Laboratory (PNNL). PNNL is a multi-program national laboratory operated for the U.S. Department of Energy (DOE) by Battelle Memorial Institute under Contract No. DE-AC05-76RL01830.

## Contents

Abstract.....	ii
Summary .....	iii
Acknowledgments.....	iv
1.0 Introduction.....	1
1.1 Heading 2 .....	1
2.0 Methods .....	3
2.1 Materials preparation .....	3
2.2 Characteristic.....	3
2.3 Electrochemical measurements .....	4
3.0 Results.....	5
3.1 Li extraction device .....	5
3.2 Li extraction validation.....	6
3.3 Direct cathode synthesis with the extracted Li.....	8
3.4 Design of Li extraction flow cell.....	10
4.0 Conclusion .....	12
5.0 References.....	13

## Figures

**Fig. 1** Li extraction device and working mechanism. A) Schematic of the Li extraction device: the cathode and anode chambers are separated by LAGP SSE. Anode is stainless steel (SS) mesh immersed in Li-containing aqueous; cathode is EMD in contact with organic electrolyte. B) Voltage-capacity curves of EMD tested in Li||EMD coin cells with different cut-off voltages. Electrolyte is 1M LiPF<sub>6</sub> in EC/EMC (w/w=3:7) and current density is 0.05C (1C = 200 mA g<sup>-1</sup>). C) Diagram of stable electrochemical window of water at pH=7 and working voltage window of different Li host materials. D, E) Evolutions of the LAGP interfacial resistances in contact with 3M LiTFSI in EC/EMC (D) and 5M LiCl (E) during the first 22.5 h, the corresponding *in-situ* impedance were inserted separately.

**Fig. 2** Voltage profiles and structural characterizations of pristine and Li-intercalated EMD. A) Voltage profile of the Li extraction device with LAGP as separator. Electrolytes filled in the anode and cathode chambers are 5M LiCl in aqueous and 3M LiTFSI in EC/EMC. B) XRD patterns of the pristine (black curve) and Li-intercalated (red curve) EMD. C-F) TEM images of pristine EMD electrode (C, D) and Li-intercalated EMD (E, F). G) Li EELS spectra of pristine and Li-intercalated EMD. H) Voltage profiles of EMD in different mixed solutions (Li/Na and Li/Mg) to verify the selectivity of LAGP, the corresponding Li-ion concentrations vary from ppm scale to 2.5 M.

**Fig. 3** Cathodes synthesis with the Li-extracted EMD and corresponding cell performance. A) XRD patterns of the synthesized spinel LiMn<sub>2</sub>O<sub>4</sub> and layered NMC333 cathodes. B, C) SEM images of LiMn<sub>2</sub>O<sub>4</sub> (B) and NMC333 (C). D, F) Long-term cycling performance of the LiMn<sub>2</sub>O<sub>4</sub> (D) and NMC333 (F), which were cycled at 0.1C for the initial formation cycles, then charged and discharged at 0.33C for the following cycles (Color fill under the curve is the error bar from 2

parallel cycles). E, G) Evolution of capacity-voltage profiles of  $\text{LiMn}_2\text{O}_4$  (E) and NMC333 (G) in the first 300 cycles.

**Fig. 4** Photo of the designed Li-extraction flow cell with a 2 in× 2 in working area (left) and the continuous operation of the Li-extraction flow cell (right).

## 1.0 Introduction

### 1.1 Heading 2

Lithium is emerging as a critical material due to its wide applications in various industries, especially driven by the quick-growing demand of Li-ion/Li batteries for portable devices, electric vehicles and grid energy storage.<sup>1, 2</sup> The global Li demand has reached 28100 metric tons (Li<sub>2</sub>CO<sub>3</sub> equivalent) in 2010 and will be expected to exceed two million metric tons by 2030.<sup>3, 4</sup> Accordingly, Li prices have surged since 2012, increasing from \$4200 to \$8000 per metric ton in 2020. Currently, commercially available Li is mainly mined from salt-lake brines and ores followed by separation/purification through chemical treatment. This approach encounters two significant challenges in practice. First, the Li reserve on land is limited and geographically uneven to meet the long-lasting and worldwide demand.<sup>5</sup> Second, the chemical sedimentation and purification processes are slow (years) and inefficient (< 50% recovery), and require heavy use of fresh water and waste treatment, which are not desirable technically and economically. As a dominant Li resource, ocean contains 2.3×10<sup>14</sup> kg Li, 50000 × more Li than on land.<sup>6</sup> Moreover, as more of our Li resources are consumed and manufactured into Li-ion batteries, growing research interests are being focused on recycling the Li from used batteries. Battery recycling combines wet chemistry and precipitation processes to dissolve the battery components into complex solutions and is being pursued despite of the high cost and environmental impacts of the process. Thus, innovation is needed to improve Li recovery from Li-containing solutions like seawater, brine, and Li-recycle solutions with minimal time and economic impacts.<sup>2, 5, 7-9</sup> Despite technical maturity of the Li production process, the conventional sedimentation processing requiring pre-concentration of brine, precipitation reagents, and post-separation of Li, are time consuming and costly. Direct Li extraction from chemically complex, low-Li waters (e.g., seawater or brines) are desirable but has been held back by the low Li concentration and interferences of other ions, such as H<sup>+</sup>/OH<sup>-</sup>, Na<sup>+</sup> and Mg<sup>2+</sup>.<sup>9-12</sup> To overcome the barriers, many novel Li extraction technologies have been proposed based on mechanisms of adsorption, nanofiltration, electrodialysis, and electrolysis. In the context of adsorption, spinel type manganese oxides<sup>13</sup> and Ti oxides Li ion sieves<sup>14</sup> have been adopted for a moderate Li/Na selectivity, however the slow Li adsorption and desorption kinetics make those approaches challenging for practical deployment. Benefiting from the high ionic conductivity and selectivity, membrane separation was employed to enrich Li from low concentration waters by using polymer-, ceramic- or glass-based separators. Hoshino proposed an electrodialysis approach for Li enrichment by using Li<sub>1+x+y</sub>Al<sub>x</sub>Ti<sub>2-x</sub>Si<sub>y</sub>P<sub>3-y</sub>O<sub>12</sub> solid membrane and obtained a 7% Li recovery after 72 h treatment.<sup>15</sup> Zhou's team developed an electrolysis method by using a Li<sub>1+x</sub>Al<sub>y</sub>Ge<sub>2-y</sub>(PO<sub>4</sub>)<sub>3</sub> solid membrane and demonstrated Li metal deposition from emulated seawater.<sup>5</sup> Recently, Lai et al. realized a continuous Li enrichment from seawater through a three-chamber design by adopting Li<sub>0.33</sub>La<sub>0.56</sub>TiO<sub>3</sub> solid membrane and anion exchange membrane<sup>16</sup>, which opens a new window for efficient Li mining. Zhao et al. extracted Li from brine by using FePO<sub>4</sub> as an adsorbent at a high energy efficiency.<sup>17</sup> However, to recover Li from LiFePO<sub>4</sub>, reverse electrochemical deintercalation is still needed, requiring electrode swapping and more power input. In addition, the deintercalated Li still stays in a form of LiCl, which needs to be converted into Li<sub>2</sub>CO<sub>3</sub> or LiOH for battery manufacturing. Moreover, continuous Li extraction methods heavily rely on the structural reversibility and durability of the Li host materials in aqueous solutions.<sup>18</sup> So, one general issue for the aforementioned Li extraction methods is that after Li is harvested, many costly steps of adsorbent regeneration and Li purification are still required to generate industry usable Li resources (e.g., Li<sub>2</sub>CO<sub>3</sub>, LiOH) or to enable repeated Li recovery. These additional steps affect overall processing efficiency and impose stiff cost and environmental penalties. For Li extraction

from the used batteries, it is always accompanied with the separation of other elements or components using physical and chemical separation processes.<sup>19-25</sup> The high-concentration Li-containing solution need to react with precipitation reagents to produce useful Li salts. Such a processing is widely applied in Li battery recycling. However, in addition to the processing cost, during the above recycle processes, some of the Li may be lost within the waste streams. Moreover, it always requires a large quantity of fresh water, causing resource and environmental problems.<sup>26</sup> Given the significant economic and environmental impacts, there is a sense of urgent growing momentum to establish a low-cost, low-pollution and efficient scheme for lithium extraction from low concentration Li-containing solutions. In this work, we demonstrate a new and generic approach that can realize Li extraction from low-Li or Li-battery recycling solutions into a low-cost and usable end-product. By directly using the extracted Li, commercial Li battery cathodes were synthesized with high phase purity. This technology is based on combined membrane electrolysis and electrochemical intercalation reactions, where a Li-ion selective membrane ( $\text{Li}_{1.5}\text{Al}_{0.5}\text{Ge}_{1.5}(\text{PO}_4)_3$ , LAGP) and low-cost electrolytic manganese dioxide (EMD) are used as the membrane and Li host, respectively. Different to previous attempts, instead of using low capacity materials such as structural reversible  $\text{FePO}_4$ , we focus on materials with high Li extraction capacity and efficiency, minimizing post-processing costs. The EMD was selected as Li host material due to its low price among the typical cathode transitional metals (Ni, Co, Mn), ability to be used directly in the synthesis of commercial cathodes, and the high specific capacity of  $308 \text{ mAh g}^{-1}$  ( $\text{MnO}_2$ ).<sup>27</sup> There are three main advantages of our technology. First, the high purity of the extracted Li. Owing to the high selectivity of the LAGP membrane, only Li ions are allowed through the membrane to intercalate into EMD, blocking other impurity metal cations or  $\text{H}^+$ . The resulting Li-EMD then has high chemical purity and can be directly used to manufacture other battery cathodes. Second, eliminated costly Li separation and refinement. The harvested Li and EMD host (Li-EMD) are precursor materials for battery cathodes and can be directly used for cathode production after adding necessary elements, depending on the design of target cathode formulas (e.g.,  $\text{LiM}_x\text{N}_y\text{Co}_z\text{O}_2$ ,  $x+y+z=1$ ). Third, high efficiency and low cost. In our approach, the absorbent regeneration and Li separation/purification that are required in other Li recovery processes are fully eliminated. So, the significant impacts of these steps on processing efficiency, energy consumption and cost are removed, making Li battery cathode production more cost competitive. The Li extraction process can be deployed by swapping the loaded EMD cartridges at a desired lithiation depth or after its full lithiation, which is easy to be automated. Moreover, the environmental impacts caused by chemical use and waste treatment associated with conventional sedimentation processes are also avoided in this method.

## 2.0 Methods

### 2.1 Materials preparation

**Li-EMD to spinel  $\text{LiMn}_2\text{O}_4$ :** Electrolytic manganese dioxide (EMD) is received from TRONOX. The lithiated EMD, named as Li-EMD, was obtained by electrochemical Li extraction technology. To synthesize spinel  $\text{LiMn}_2\text{O}_4$ , the Li content (x) in  $\text{Li}_x\text{MnO}_2$  was controlled less than 0.5 by controlling the discharge time under the condition of the known theoretical capacity and the settled current density. After the electrode was washed and dried out, the electrode material was scraped off with a blade and calcined in air at 500 °C for 4h. For more Li-EMD materials, new EMD electrode will be prepared and applied for lithium extraction. Based on the ICP-OES analysis,  $\text{Li}_2\text{CO}_3$  was used to adjust the Li/Mn to 0.5 when needed. The mixture was grounded, pressed into pellet, and calcined at 900 °C for 12 h under oxygen atmosphere, the corresponding heating and cooling temperature were set as 5 °C  $\text{min}^{-1}$  and 2 °C  $\text{min}^{-1}$ . Finally, a dark powder is obtained, which is spinel  $\text{LiMn}_2\text{O}_4$ .

**Li-EMD to  $\text{LiNi}_{1/3}\text{Co}_{1/3}\text{Mn}_{1/3}\text{O}_2$ :**  $\text{Ni}(\text{NO}_3)_2 \cdot 6\text{H}_2\text{O}$ ,  $\text{Co}(\text{NO}_3)_2 \cdot 6\text{H}_2\text{O}$  and  $\text{LiOH} \cdot \text{H}_2\text{O}$  were purchased from Sigma. The lithiated EMD ( $\text{Li}_{0.77}\text{MnO}_2$ ) powder was scraped off and mixed with  $\text{Ni}(\text{NO}_3)_2 \cdot 6\text{H}_2\text{O}$  and  $\text{Co}(\text{NO}_3)_2 \cdot 6\text{H}_2\text{O}$  in molar ratio of 1:1:1. Meanwhile, according to the Li content in Li-EMD, a certain amount of  $\text{LiOH} \cdot \text{H}_2\text{O}$  was added into the above solid mixture to tune the ratio of  $[(\text{Li}_{\text{Li-EMD}} + \text{Li}_{\text{LiOH}}) : (\text{Ni} + \text{Co} + \text{Mn})]$  to 1.04 : 1. The 4 mol% excess Li is used to compensate the Li loss during calcinating. The final mixture was grounded and pre-calcinated at 500 °C for 4 h, and then grounded in mortar, followed by heating at 900 °C for 6h in air. The ramping rate was controlled at 5 °C  $\text{min}^{-1}$  for both heating and cooling. The final dark powder is  $\text{LiNi}_{1/3}\text{Co}_{1/3}\text{Mn}_{1/3}\text{O}_2$ , labelled as NMC333.

**$\text{Li}_{1.5}\text{Al}_{0.5}\text{Ge}_{1.5}(\text{PO}_4)_3$  synthesizing and characterization:**  $\text{Li}_{1.5}\text{Al}_{0.5}\text{Ge}_{1.5}(\text{PO}_4)_3$  (LAGP) material was obtained from Ampcera. The powder had a mean particle size of approximately 500 nm. Disks were uniaxially pressed in a 31.7 mm die with 5000 lbs applied force (4087 psi or about 28 MPa) for 30 seconds. The resulting pellets were placed in an MgO tray and covered with sacrificial powder of the same composition. The tray was closed with an MgO lid. The samples were fired in air with a heating rate of 1 °C  $\text{minute}^{-1}$  to 850 °C, held for 4 hours, and cooled to room temperature at 5 °C  $\text{minute}^{-1}$ . The prepared LAGP (25 cm in diameter) presents a very dense structure. Before testing, the interfacial stability between LAGP and applied electrolytes (SE/LE-interface), including organic and aqueous electrolytes, was measured by *in-situ* impedance. For LAGP/liquid electrolyte (LE) compatibility test, one side of LAGP was coated with Au and connected with SS-rod, the other uncoated fresh side contacted with liquid electrolytes. There are two semicircles. The high-frequency semicircle has not totally shown up under 1 MHz, which can be allocated to the intragrain transport resistance ( $R_{SE,bulk}$ ) and intergrain transport resistance ( $R_{SE,gb}$ ). The middle-frequency semicircle is related to the LAGP/LE-interface resistance. The overall ionic conductivity of LAGP is around 0.49 mS  $\text{cm}^{-1}$ .

### 2.2 Characteristic

The morphology of the materials was studied by scanning electron microscopy (SEM, JSM-IT2000). The crystal structure of our synthesized materials before and after Li extraction were analyzed by X-ray diffraction (XRD, Rigaku MiniFlex 600) in a 2-theta range of 10° - 80° using Cu  $\text{K}\alpha$  radiation operated at 40 kV and 15 mA. Li content in the materials was analyzed by an inductively coupled plasma-optical emission spectrometer (ICP-OES) (PerkinElmer Optima 7300 DV). TEM samples were prepared by dispensing the cathode particles onto TEM lacey carbon grids inside an Ar-filled glovebox. TEM imaging was conducted on a Titan 80-300™ scanning/transmission electron microscope operated at 300 kV. STEM EELS microanalysis data

were collected on an aberration corrected JEOL GrandARM-300F with the operation voltage of 300 kV, and a post-column Gatan Image Filter (GIF) working at 0.25 eV/channel energy dispersion.

## 2.3 Electrochemical measurements

Three cell configurations were employed for the materials validation and technology demonstration, including traditional coin-cell, liquid/LAGP/liquid-electrolyte cell and 3-electrode cell.

Coin-cell configuration with sandwiched anode/separator/cathode structure was used for fast material evaluation, where organic based Li solution of 1M LiPF<sub>6</sub> in ethyl carbonate (EC) and ethyl methyl carbonate (EMC) (3:7 by weight), Li metal and active material (EMD, LiMn<sub>2</sub>O<sub>4</sub> or NMC333) were used as electrolyte, anode, and cathode, respectively. The applied electrolyte content is 70  $\mu$ L and the corresponding Li-metal thickness is 450  $\mu$ m. EMD electrode was prepared by mixing electrode materials, PVDF and conductive carbon with a ratio of 80:10:10, and the mixing ratio in LiMn<sub>2</sub>O<sub>4</sub> and NMC333 electrodes is 70:20:10. All the prepared coin-cells are tested at 30 °C.

The cell with LAGP is composed of multilayer structures, namely anode/aqueous-electrolyte/LAGP/organic-electrolyte/cathode, the corresponding aqueous electrolyte and organic electrolyte are Li-containing (5M LiCl) aqueous and 3M LiTFSI in EC/EMC (w/w=3:7), respectively. Stainless steel rod and EMD electrode were applied as anode and cathode, the corresponding EMD electrode loading is around 4 mg cm<sup>-2</sup>. The electrolyte contents of 5M LiCl and 3M LiTFSI used in this setup are 1 mL and 75  $\mu$ L, respectively. The mass of the applied LAGP is around 1.2g.

In 3-electrode cell, we developed a solvent assisted solid processing method to prepare free-standing EMD electrode and control the electrode architecture without sacrificing electrode stability/durability. The free-standing EMD electrode was attached onto Ti mesh current collector, forming the Li extraction film electrode, and the corresponding counter electrode is Pt. The used reference electrodes are Ag/AgCl electrode (in aqueous) or Ag/Ag<sup>+</sup> electrode (in organic electrolyte). The testing voltage in three-electrode cell was set between open circuit voltage (OCV) and -0.54 V, and the corresponding current density is 0.1C (1C=200 mA g<sup>-1</sup>).

## 3.0 Results

### 3.1 Li extraction device

The schematic of the proposed Li extraction device is shown in **Fig. 1A**. The Li extraction device was divided into anode and cathode chambers by the LAGP membrane, and the chambers are filled with Li containing aqueous solution and nonaqueous electrolyte. Stainless steel (SS) is set in anode chamber, and the EMD was filled in the cathode chamber in a form of either processed film or powders. When an electric field is applied, current flow will be generated and sustained by the anodic and cathodic reactions and the Li ion transportation through the LAGP membrane. Driven by electric field, Li ions in anode chamber will pass through the LAGP membrane and intercalate into the EMD, forming Li-EMD (Equation 1 in Fig. 1A); the Cl<sup>-</sup> in anode chamber will be oxidized to Cl<sub>2</sub> for charge balance (Equation 2 in Fig. 1A). Through this circuit loop, Li ions will be continuously extracted out from feed stream into EMD at a speed controlled by applied current. To realize such design, two key prerequisites should be met.

First, Li interaction voltage and capacity should fit the device design. As shown in **Fig. 1B**, EMD has a discharge plateau ranged from 2.5 V to 3.25 V vs. Li, which corresponds to -0.54 V - 0.21 V vs. SHE in a solution with pH=7 (**Fig. 1C**). Majority of the electrochemical platform falls well into a stable electrochemical window of water. The Li intercalation capacity in EMD was verified in Li||EMD coin cells by using the EMD electrode and nonaqueous electrolyte. Capacities of 188, 250 and 276 mAh g<sup>-1</sup> were obtained with discharge cutoff voltages of 2.7, 2.0, and 1.5 V vs. Li, respectively, confirming high Li intercalation capacity of the EMD (Fig. 1B).

Second, stability of LAGP against aqueous solution and nonaqueous electrolyte should also be verified before device deployment. Accordingly, bulk and interfacial stability of LAGP when contacted with aqueous solutions (5M LiCl/H<sub>2</sub>O) and nonaqueous electrolyte (3M LiTFSI/EC/EMC) were monitored by *in-situ* EIS using a hybrid cell design. Initially, the LAGP has some interactions with both solutions as proved by the variation of interfacial resistance ( $R_{LE/SE}$ ) (**Fig. 1D and E**), which is consistent with previous reports.<sup>28, 29</sup> It is interesting that the LAGP interface is stabilized after exposure for 3.7 h in nonaqueous electrolyte (Fig. 1D) and 7.5 h in aqueous solution (Fig. 1E), which was due to the surface passivation of LAGP.<sup>28</sup>

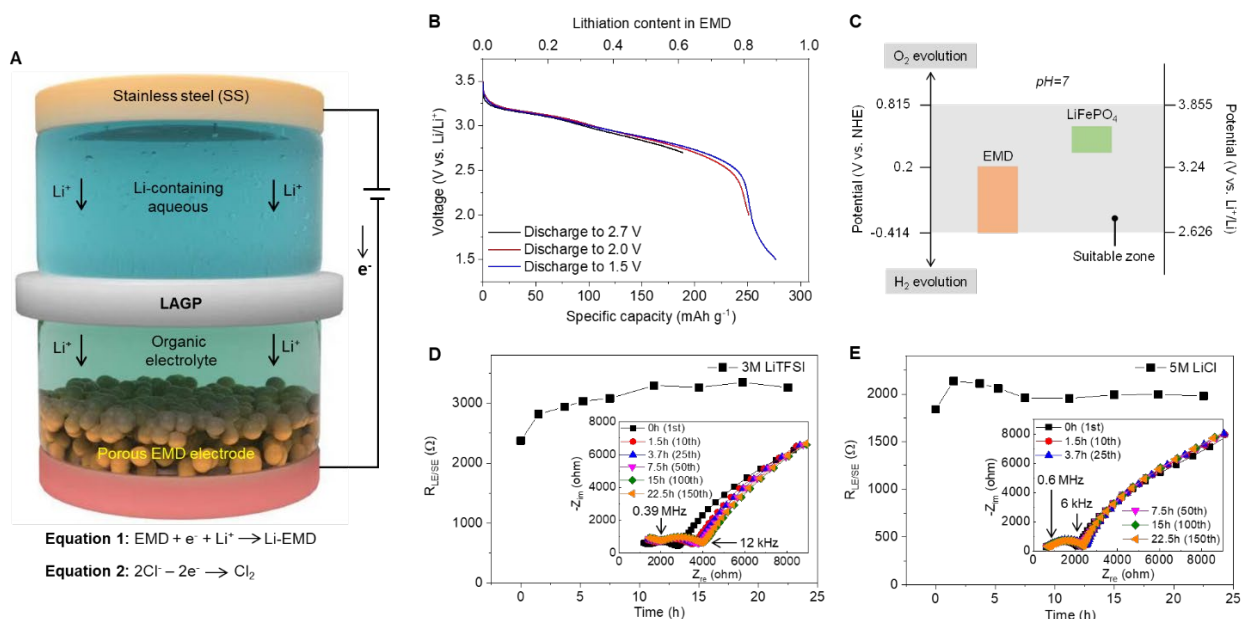


Fig. 1 Li extraction device and working mechanism. A) Schematic of the Li extraction device: the cathode and anode chambers are separated by LAGP SSE. Anode is stainless steel (SS) mesh immersed in Li-containing aqueous; cathode is EMD in contact with organic electrolyte. B) Voltage-capacity curves of EMD tested in Li||EMD coin cells with different cut-off voltages. Electrolyte is 1M LiPF<sub>6</sub> in EC/EMC (w/w=3:7) and current density is 0.05C (1C = 200 mA g<sup>-1</sup>). C) Diagram of stable electrochemical window of water at pH=7 and working voltage window of different Li host materials. D, E) Evolutions of the LAGP interfacial resistances in contact with 3M LiTFSI in EC/EMC (D) and 5M LiCl (E) during the first 22.5 h, the corresponding in-situ impedance were inserted separately.

### 3.2 Li extraction validation

Li extraction was demonstrated by applying a constant current density of 10 mA g<sub>EMD</sub><sup>-1</sup>. Due to limited volume of the anode chamber, Li solution with a relatively high concentration (5M LiCl/H<sub>2</sub>O) was used to increase utilization rate of the EMD. **Fig. 2A** exhibits voltage response upon Li intercalation. With more Li intercalation into EMD, the voltage curve decreased slowly at the beginning and dropped quickly at the end, showing a plateau at around -0.1 vs. Ag/AgCl. The overall Li intercalation capacity was 220 mAh g<sup>-1</sup>, corresponding to 71.4% recovery efficiency calculated by actual Li extraction capacity/theoretical EMD capacity. The presented extraction capacity means 0.772 mol of Li can be harvested by 1 mol EMD if all Mn ions are assumed at a 4+ valence, which is consistent with the elemental analysis result (via inductively coupled plasma-optical emission spectrometry (ICP-OES)) of the lithiated EMD, where the actual Li/Mn atomic ratio was measured to be 0.816, suggesting Li adsorption or exchange may coexist during the electrochemical extraction.<sup>30</sup> To further confirm the Li intercalate into EMD crystal structure, X-ray Diffraction (XRD) and high-resolution transmission electron microscopy (TEM) characterization were performed on EMD before and after Li extraction process. XRD results indicate that after extraction processing the EMD experienced a significant structural change and transforms to an orthorhombic Li<sub>x</sub>MnO<sub>2</sub> structure (**Fig. 2B**). This phase change was induced by reorganization of Mn local structures accompanying its valent change and Li intercalation, which is proved by high resolution TEM (HRTEM) (**Fig. 2C-F**). It's well known EMD has a crystal structure of γ-MnO<sub>2</sub>, which consists of the intergrowth of pyrolusite and ramsdellite, and the lattice fringes with d-spacing of 0.186 nm were clearly observed and assigned to the (131) plane of γ-MnO<sub>2</sub> (**Fig. 2C,D**).<sup>31</sup> After Li intercalation, new lattice fringes at d=0.359 were observed, which is a characteristic (201) plane of orthorhombic Li<sub>x</sub>MnO<sub>2</sub> (**Fig. 2E,F**), matching with the XRD analysis (**Fig. 2B**). Moreover, in electron energy lose spectroscopy (EELS), a broad peak was observed in Li-EMD (**Fig. 2G**), further confirming the existence of Li in the intercalated EMD.<sup>32</sup> After Li extraction, structural and morphological evolution of the tested LAGP were characterized. The SEM/EDS results indicate that the LAGP is stable against 5M LiCl aqueous solution.

The selective Li extraction from the aqueous Li stream and successful intercalation of Li<sup>+</sup> into EMD are achieved by using the nonaqueous electrolyte and LAGP membrane, which play a key role in removing the potential interferences of H<sup>+</sup> and other cations. If aqueous electrolyte was used in the cathode chamber, competitive intercalations between Li<sup>+</sup> and H<sup>+</sup> were identified. At the first glance, the Li extraction voltage-capacity curve in a 3-electrode system is very similar to the behaviors in nonaqueous electrolyte (**Fig. 2A**) and the discharge capacity was 285 mAh g<sup>-1</sup>, likely suggesting large-capacity Li extraction. However, XRD analysis and HRTEM images indicate a completely different phase evolution pathway. Instead of forming Li-EMD, a phase of MnO(OH) was observed at the end of process, which is similar to observations in primary MnO<sub>2</sub> batteries<sup>33</sup> and ascribed to the H<sup>+</sup> (or H<sub>3</sub>O<sup>+</sup>) intercalation. The Li/Mn ratio measured by ICP is as low as 0.018, confirming H<sup>+</sup> intercalation dominates the EMD conversion due to its smaller polarization and diffusion energy barrier. Decreasing the H<sup>+</sup> concentration or increasing Li<sup>+</sup>

concentration help to increase  $\text{Li}^+$  intercalation capacity to some extent, further confirming the competitions between the  $\text{Li}^+$  and  $\text{H}^+$ . By using a nonaqueous electrolyte,  $\text{H}^+$  co-intercalation can be fully eliminated. Meanwhile, the LAGP membrane functions effectively to prevent metal cations from co-intercalation into the EMD. If the  $\text{Na}^+$  and  $\text{Mg}^{2+}$ , typical cations in seawater and brines, exist in the cathode chamber, they will co-intercalate into EMD crystal if without using LAGP membrane, causing ion impurities in final products and lowering Li extraction efficiency. With help of the LAGP membrane, those cations are fully blocked. As shown in **Fig. 2H**, with  $\text{Li}/\text{Na}=1$  and  $\text{Li}/\text{Mg}=1$ , the EMD has very similar Li-extraction behaviors. Even when the Li/M ratio was decreased to an extremely low level as those in seawater (0.45  $\mu\text{m}$  filtered seawater from Sequim Bay, WA, USA), the Li intercalation in EMD still happened although higher polarization voltage and smaller capacities were observed. The observed low specific capacities in low Li concentration solutions are due to the limited total Li amount in solutions in comparison with the high mass loading EMD electrodes. The corresponding Li recovery efficiency in 5M NaCl with 17.5 ppm LiCl is around 89.2%. The LAGP after tested in 5M NaCl with 17.5 ppm Li and 1M  $\text{MgCl}_2$  with 29.4 ppm Li maintained the same structure and morphology as the pristine LAGP. The EDS results indicate that high concentration of  $\text{MgCl}_2$  has little effect on surface composition of the LAGP, while a slight enrichment of  $\text{Na}^+$  in LAGP was observed after test in the NaCl based solution. This indicates exchange of  $\text{Li}^+$  with  $\text{Na}^+$ , which however has little effect on the structure of the LAGP. After the Li extraction test in 5M NaCl with 17.5 ppm Li, the LAGP still functioned well for Li extraction without degradation of Li extraction capacity.

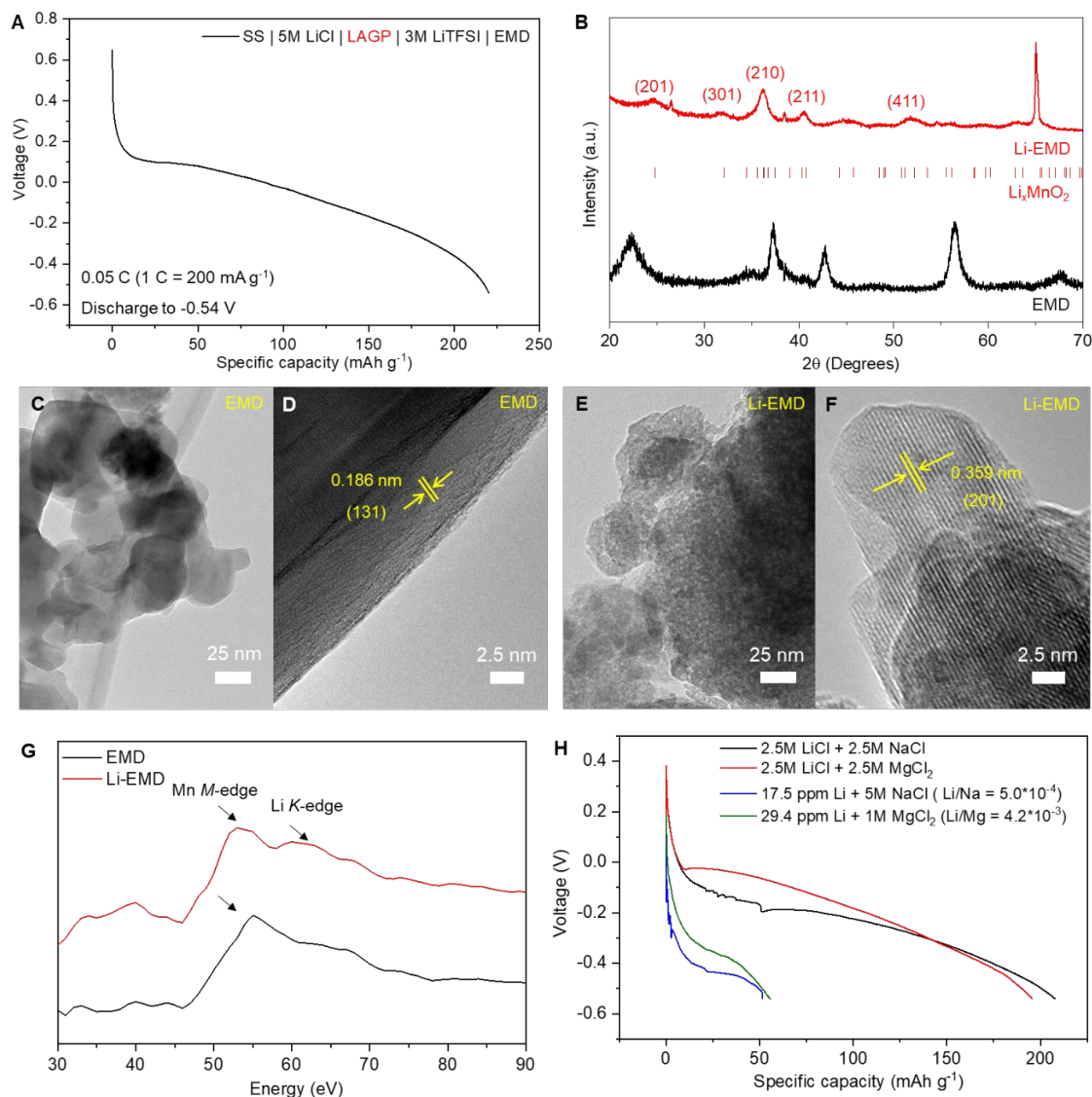


**Fig. 2** Voltage profiles and structural characterizations of pristine and Li-intercalated EMD. A) Voltage profile of the Li extraction device with LAGP as separator. Electrolytes filled in the anode and cathode chambers are 5M LiCl in aqueous and 3M LiTFSI in EC/EMC. B) XRD patterns of the pristine (black curve) and Li-intercalated (red curve) EMD. C-F) TEM images of pristine EMD electrode (C, D) and Li-intercalated EMD (E, F). G) Li EELS spectra of pristine and Li-intercalated EMD. H) Voltage profiles of EMD in different mixed solutions (Li/Na and Li/Mg) to verify the selectivity of LAGP, the corresponding Li-ion concentrations vary from ppm scale to 2.5 M.

### 3.3 Direct cathode synthesis with the extracted Li

The Li-EMD was obtained after successfully addressing the interferences of  $H^+$  and metal cations. The Li and Mn of the harvested Li-EMD are precursor materials of many Li battery cathodes and thus can be used for direct cathode production. Depending on the target cathode formulas, the Li-EMD can be used as the sole precursor or mixed with additional transition metal or Li resources.<sup>34-36</sup> For instance,  $Li_{0.5}MnO_2$  can be processed through the extraction device by

controlling Li intercalation content and then is used to prepared spinel  $\text{LiMn}_2\text{O}_4$  by high-temperature calcination. For another category of Li-ion cathodes layered transition metal oxides, taking  $\text{LiNi}_{1/3}\text{Mn}_{1/3}\text{Co}_{1/3}$  (NMC333) as an example, addition metal precursors of Ni and Co will be mixed with Li-EMD first, and then calcinated into the target cathode by controlling the heating temperature or atmosphere. **Fig. 3A-C** show the phase structure and morphology of the synthesized spinel  $\text{LiMn}_2\text{O}_4$  and layered NMC333. The synthesized  $\text{LiMn}_2\text{O}_4$  has a spinel cubic structure with space group  $\text{Fd}\bar{3}\text{m}$  (Fig. 3A) and a diamond-shaped morphology with sharp edges (Fig. 3B), which are typical for the material. For NMC333, all the diffraction peaks can be indexed to layered hexagonal structure of  $\alpha\text{-NaFeO}_2$  with space group  $\text{R}\bar{3}\text{m}$ . Observation of the clear splitting of peak (006)/(012) and (018)/(110) indicates a well grown crystals with layered structures, which is consistent with the morphology characterization (Fig. 3C). The electrochemical properties of both cathodes were tested in coin cells by coupling with Li metal anode and organic electrolyte (**Fig. 3D-G**). The spinel  $\text{LiMn}_2\text{O}_4$  exhibits a typical two-plateau charge/discharge profiles with a reversible of  $92.8 \text{ mAh g}^{-1}$  at 0.1C. The cell has an exceptional cycling stability in terms of capacity and discharging voltage at 0.33C and demonstrates a capacity retention of 97.7% after 300 cycles. For NMC333, within a voltage range of 2.7-4.5 V, a reversible capacity of  $139.4 \text{ mAh g}^{-1}$  was obtained. The capacity retention at 0.33 C is 74.4% after 300 cycles. The obtained discharge specific capacities of  $\text{LiMn}_2\text{O}_4$  and NMC333 are slightly lower than the commercial ones, which may be attributed to the complex of Li-EMD precursor, bringing hindrance for Li-ion diffusion kinetics.<sup>37, 38</sup> The capacity decay in NMC333 is associated with voltage drop, which was due to the exaggerated side reactions of materials with electrolyte caused by the small particle size.<sup>39, 40</sup> To improve the cycling stability for commercial cells, such small particles need to be remanufactured into large size secondary particles or big single-crystalline materials.<sup>41, 42</sup> This demonstration shows successful conversion of Li extracted from an aqueous source being converted to a usable battery material without the need for extensive post-processing.

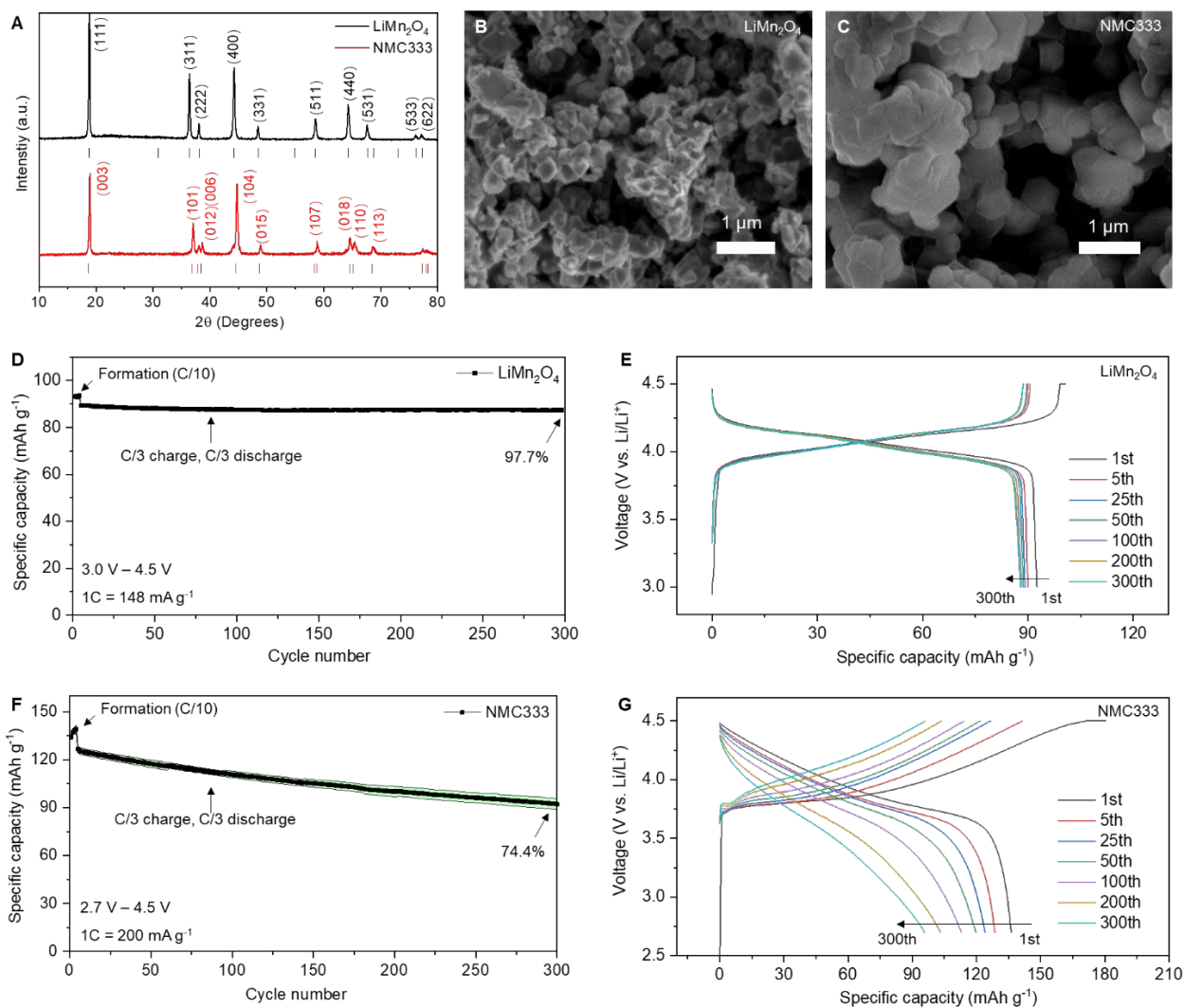


**Fig. 3** Cathodes synthesis with the Li-extracted EMD and corresponding cell performance. **A)** XRD patterns of the synthesized spinel  $\text{LiMn}_2\text{O}_4$  and layered NMC333 cathodes. **B,** **C)** SEM images of  $\text{LiMn}_2\text{O}_4$  (**B**) and NMC333 (**C**). **D, F)** Long-term cycling performance of the  $\text{LiMn}_2\text{O}_4$  (**D**) and NMC333 (**F**), which were cycled at 0.1C for the initial formation cycles, then charged and discharged at 0.33C for the following cycles (Color fill under the curve is the error bar from 2 parallel cycles). **E, G)** Evolution of capacity-voltage profiles of  $\text{LiMn}_2\text{O}_4$  (**E**) and NMC333 (**G**) in the first 300 cycles.

### 3.4 Design of Li extraction flow cell

To validate the Li extraction approach for practical use, a new Li extraction flow cell was designed and machined, and stable operation of flow cell was demonstrated. Under this effort: 1) the Li extraction cell with working area  $> 2 \text{ in} \times 2 \text{ in}$  was designed and a new sealing mechanism was developed and deployed. 2) A large size ceramic Li-ion selective membrane with size of  $2 \text{ in} \times 2 \text{ in}$  was prepared and integrated with the new reactor design. 3) Large size EMD electrodes were fabricated and integrate with the new reactor design. and 4) The flow cell was operated

continuously for 3 days without seeing cell failure or break of ceramics membrane. Further research is in progress by using the flow cell design and real lake brines.



Fig. 4 Photo of the designed Li-extraction flow cell with a 2 in× 2 in working area (left) and the continuous operation of the Li-extraction flow cell (right).

## 4.0 Conclusion

We developed a combined Li extraction-utilization technology to realize efficient Li recovery from Li-containing aqueous solutions for direct cathode preparation without processes of Li separation and refinement. By eliminating the interferences of  $H^+$  and other metal cations through this approach, Li can be selectively extracted and inserted into EMD host, generating a chemically pure Li and Mn resource. High Li recovery efficiency of 0.772 Li/EMD was achieved. Instead of requiring post-processing Li separation or Li-host regeneration, the harvested Li along with the EMD can be used directly for Li battery cathode production. The synthesized spinel  $LiMn_2O_4$  and NMC333 were pure in phase structure and exhibit decent electrochemical performance as promising cathode materials. Significant benefits of using this technical loop for Li recovery and utilization include selective Li extraction, eliminated post-treatment, and high efficiency, which are desirable for industrial deployment. The Li-extraction flow cell with large working area was designed, manufactured, and demonstrated for continuous operation. This Li recovery and utilization technology could be expected to address the existing challenges of Li shortage and battery cost, supporting the vehicle electrification and decarbonization of socioeconomic system.

## 5.0 References

- (1) Swain, B., Recovery and recycling of lithium: a review. *Sep. Purif. Tech.* **2017**, 172, 388-403.
- (2) Lang, J., Y. Jin, K. Liu, Y. Long, H. Zhang, L. Qi, H. Wu, and Y. Cui, High-purity electrolytic lithium obtained from low-purity sources using solid electrolyte. *Nat. Sustain.* **2020**, 3, 386-390.
- (3) Garside, M. *Global lithium mine production 2010-2021*. Feb 28, 2022; Available from: <https://www.statista.com/statistics/606684/world-production-of-lithium/>.
- (4) Garside, M. *Global projection of total lithium demand 2019-2030*. Mar 4, 2022; Available from: <https://www.statista.com/statistics/452025/projected-total-demand-for-lithium-globally/>.
- (5) Yang, S., F. Zhang, H. Ding, P. He, and H. Zhou, Lithium metal extraction from seawater. *Joule* **2018**, 2, 1648-1651.
- (6) Bardi, U., Extracting minerals from seawater: an energy analysis. *Sustainability* **2010**, 2, 980-992.
- (7) Ryu, T., J. Shin, S.M. Ghoreishian, K.-S. Chung, and Y.S. Huh, Recovery of lithium in seawater using a titanium intercalated lithium manganese oxide composite. *Hydrometallurgy* **2019**, 184, 22-28.
- (8) Xu, X., Y. Zhou, Z. Feng, N.U. Kahn, Z.U. Haq Khan, Y. Tang, Y. Sun, P. Wan, Y. Chen, and M. Fan, A self-supported  $\gamma$ -MnO<sub>2</sub> film electrode used for electrochemical lithium recovery from brines. *Chempluschem* **2018**, 83, 521-528.
- (9) Liu, C., Y. Li, D. Lin, P.-C. Hsu, B. Liu, G. Yan, T. Wu, Y. Cui, and S. Chu, Lithium extraction from seawater through pulsed electrochemical intercalation. *Joule* **2020**, 4, 1459-1469.
- (10) Choubey, P.K., K.-S. Chung, M.-s. Kim, J.-c. Lee, and R.R. Srivastava, Advance review on the exploitation of the prominent energy-storage element Lithium. Part II: From sea water and spent lithium ion batteries (LIBs). *Miner. Eng.* **2017**, 110, 104-121.
- (11) Zhao, Z., X. Si, X. Liu, L. He, and X. Liang, Li extraction from high Mg/Li ratio brine with LiFePO<sub>4</sub>/FePO<sub>4</sub> as electrode materials. *Hydrometallurgy* **2013**, 133, 75-83.
- (12) Kanoh, H., K. Ooi, Y. Miyai, and S. Katoh, Electrochemical recovery of lithium ions in the aqueous phase. *Sep. Sci. Technol.* **1993**, 28, 643-651.
- (13) Zhang, Q.-H., S. Sun, S. Li, H. Jiang, and J.-G. Yu, Adsorption of lithium ions on novel nanocrystal MnO<sub>2</sub>. *Chem. Eng. Sci.* **2007**, 62, 4869-4874.
- (14) Wang, S., P. Li, X. Zhang, S. Zheng, and Y. Zhang, Selective adsorption of lithium from high Mg-containing brines using H<sub>x</sub>TiO<sub>3</sub> ion sieve. *Hydrometallurgy* **2017**, 174, 21-28.
- (15) Hoshino, T., Innovative lithium recovery technique from seawater by using world-first dialysis with a lithium ionic superconductor. *Desalination* **2015**, 359, 59-63.
- (16) Li, Z., C. Li, X. Liu, L. Cao, P. Li, R. Wei, X. Li, D. Guo, K.-W. Huang, and Z. Lai, Continuous electrical pumping membrane process for seawater lithium mining. *Energy Environ. Sci.* **2021**, 14, 3152-3159.
- (17) He, L., W. Xu, Y. Song, Y. Luo, X. Liu, and Z. Zhao, New insights into the application of lithium-ion battery materials: selective extraction of lithium from brines via a rocking-chair lithium-ion battery system. *Glob. Chall.* **2018**, 2, 1700079.
- (18) Liu, X., X. Chen, L. He, and Z. Zhao, Study on extraction of lithium from salt lake brine by membrane electrolysis. *Desalination* **2015**, 376, 35-40.
- (19) Sommerville, R., J. Shaw-Stewart, V. Goodship, N. Rowson, and E. Kendrick, A review of physical processes used in the safe recycling of lithium ion batteries. *Sustain. Mater. Techno.* **2020**, 25, e00197.
- (20) Huang, B., Z. Pan, X. Su, and L. An, Recycling of lithium-ion batteries: Recent advances and perspectives. *J. Power Sources* **2018**, 399, 274-286.
- (21) Ordoñez, J., E.J. Gago, and A. Girard, Processes and technologies for the recycling and recovery of spent lithium-ion batteries. *Renew. Sust. Energy Rev.* **2016**, 60, 195-205.
- (22) Costa, C.M., J.C. Barbosa, R. Gonçalves, H. Castro, F. Del Campo, and S. Lanceros-Méndez, Recycling and environmental issues of lithium-ion batteries: Advances, challenges and opportunities. *Energy Storage Mater.* **2021**, 37, 433-465.
- (23) Elwert, T., D. Goldmann, F. Römer, M. Buchert, C. Merz, D. Schueler, and J. Sutter, Current developments and challenges in the recycling of key components of (hybrid) electric vehicles. *Recycling* **2015**, 1, 25-60.

- (24) Chen, X., C. Luo, J. Zhang, J. Kong, and T. Zhou, Sustainable Recovery of Metals from Spent Lithium-Ion Batteries: A Green Process. *ACS Sustainable Chem. Eng.* **2015**, *3*, 3104-3113.
- (25) Gao, W., X. Zhang, X. Zheng, X. Lin, H. Cao, Y. Zhang, and Z. Sun, Lithium Carbonate Recovery from Cathode Scrap of Spent Lithium-Ion Battery: A Closed-Loop Process. *Environ. Sci. Technol.* **2017**, *51*, 1662-1669.
- (26) Kim, S., J. Lee, S. Kim, S. Kim, and J. Yoon, Electrochemical Lithium Recovery with a LiMn<sub>2</sub>O<sub>4</sub>-Zinc Battery System using Zinc as a Negative Electrode. *Energy Technol.* **2018**, *6*, 340-344.
- (27) Huang, J., Z. Wang, M. Hou, X. Dong, Y. Liu, Y. Wang, and Y. Xia, Polyaniline-intercalated manganese dioxide nanolayers as a high-performance cathode material for an aqueous zinc-ion battery. *Nat. Commun.* **2018**, *9*, 2906.
- (28) Busche, M.R., T. Drossel, T. Leichtweiss, D.A. Weber, M. Falk, M. Schneider, M.L. Reich, H. Sommer, P. Adelhelm, and J. Janek, Dynamic formation of a solid-liquid electrolyte interphase and its consequences for hybrid-battery concepts. *Nat. Chem.* **2016**, *8*, 426-434.
- (29) Liu, J., X. Gao, G.O. Hartley, G.J. Rees, C. Gong, F.H. Richter, J. Janek, Y. Xia, A.W. Robertson, L.R. Johnson, and P.G. Bruce, The interface between Li<sub>6.5</sub>La<sub>3</sub>Zr<sub>1.5</sub>Ta<sub>0.5</sub>O<sub>12</sub> and liquid electrolyte. *Joule* **2020**, *4*, 101-108.
- (30) Biswal, A., B.C. Tripathy, K. Sanjay, T. Subbaiah, and M. Minakshi, Electrolytic manganese dioxide (EMD): a perspective on worldwide production, reserves and its role in electrochemistry. *RSC Adv.* **2015**, *5*, 58255-58283.
- (31) Wolff, P.M.D., Interpretation of some  $\gamma$ -MnO<sub>2</sub> diffraction patterns. *Acta Cryst.* **1959**, *12*, 341.
- (32) Wang, Z., D. Santhanagopalan, W. Zhang, F. Wang, H.L. Xin, K. He, J. Li, N. Dudney, and Y.S. Meng, In situ STEM-EELS observation of nanoscale interfacial phenomena in all-solid-state batteries. *Nano Lett.* **2016**, *16*, 3760-7.
- (33) Chabre, Y. and J. Parmentier, Structural and electrochemical properties of the proton/ $\gamma$ -MnO<sub>2</sub> system. *Prog. S&dSf. Chem.* **1995**, *23*, 1-130.
- (34) Wan, C., Y. Nuli, J. Zhuang, and Z. Jiang, Synthesis of spinel LiMn<sub>2</sub>O<sub>4</sub> using direct solid state reaction. *Mater. Lett.* **2002**, *56*, 357-363.
- (35) Zhao, Y.-q., Q.-l. Jiang, W.-g. Wang, D. Ke, and G.-r. Hu, Effect of electrolytic MnO<sub>2</sub> pretreatment on performance of as-prepared LiMn<sub>2</sub>O<sub>4</sub>. *T. Nonferr. Metal. Soc.* **2012**, *22*, 1146-1150.
- (36) Bao, S.-J., C.-M. Li, H.-L. Li, and J.H. Luong, Morphology and electrochemistry of LiMn<sub>2</sub>O<sub>4</sub> optimized by using different Mn-sources. *J. power sources* **2007**, *164*, 885-889.
- (37) Wu, X.M., J.L. Liu, S. Chen, F.R. Mai, and C.A. Li, Comparative study of LiNi<sub>0.05</sub>Mn<sub>1.95</sub>O<sub>4</sub> powders prepared by different materials for Li-ion battery. *Ionics* **2012**, *18*, 579-582.
- (38) Momchilov, A., V. Manev, and A. Nassalevska, Rechargeable lithium battery with spinel-related MnO<sub>2</sub> II. Optimization of the LiMn<sub>2</sub>O<sub>4</sub> synthesis conditions. *J. Power Sources* **1993**, *41*, 305-314.
- (39) Yan, P., J. Zheng, J. Liu, B. Wang, X. Cheng, Y. Zhang, X. Sun, C. Wang, and J.-G. Zhang, Tailoring grain boundary structures and chemistry of Ni-rich layered cathodes for enhanced cycle stability of lithium-ion batteries. *Nat. Energy* **2018**, *3*, 600-605.
- (40) Hu, J., L. Li, E. Hu, S. Chae, H. Jia, T. Liu, B. Wu, Y. Bi, K. Amine, C. Wang, J. Zhang, J. Tao, and J. Xiao, Mesoscale-architecture-based crack evolution dictating cycling stability of advanced lithium ion batteries. *Nano Energy* **2021**, *79*, 105420.
- (41) Hwang, I., C.W. Lee, J.C. Kim, and S. Yoon, Particle size effect of Ni-rich cathode materials on lithium ion battery performance. *Mater. Res. Bull.* **2012**, *47*, 73-78.
- (42) Bi, Y., J. Tao, Y. Wu, L. Li, Y. Xu, E. Hu, B. Wu, J. Hu, C. Wang, J.-G. Zhang, Y. Qi, and J. Xiao, Reversible planar gliding and microcracking in a single-crystalline Ni-rich cathode. *Science* **2020**, *370*, 1313-1317.

# **Pacific Northwest National Laboratory**

902 Battelle Boulevard  
P.O. Box 999  
Richland, WA 99354

1-888-375-PNNL (7665)

***[www.pnnl.gov](http://www.pnnl.gov)***